JAAS

ROYAL SOCIETY OF CHEMISTRY

PAPER

View Article Online
View Journal

Cite this: DOI: 10.1039/d3ja00308f

A potential stibnite reference material for sulfur isotope determination by LA-MC-ICP-MS

Zhi-hui Dai, *[a] Shan-ling Fu,*[a] Yue-fu Liu,[b] Yu-miao Meng,[a] Zhi-an Bao,[c] Ke-jun Hou[d] and Ting-guang Lan[a]

The identification of metal and sulfur sources in hydrothermal Sb ore deposits has long been recognized as a challenging task. Stibnite is commonly found as one of the primary ore minerals in most antimony deposits, and it can even occur as the sole ore mineral in some large antimony deposits; therefore, the sulfur isotope composition of stibnite often contains invaluable information for exploring the origin and ore-forming processes of Sb deposits. A well-characterized and matrix-matched material is imperative for conducting *in situ* S isotope microanalysis. However, the lack of standardized materials for stibnite hinders precise determination of sulfur isotope composition, thereby impeding the application of stibnite sulfur isotopes in deciphering the ore genesis of Sb deposits. The present study recommends the utilization of a natural stibnite (BJ-Snt) as a potential reference material for S isotope analysis employing laser ablation multicollector inductively coupled plasma-mass spectrometry (LA-MC-ICP-MS). The sulfur isotope compositions, backscattered electron (BSE) maps, mineral phases, and elemental compositions were analyzed to evaluate the homogeneity of the stibnite BJ-Snt. The method validation was conducted through comparison of S isotope values obtained by LA-MC-ICP-MS and IRMS, as well as intercomparisons with two other laboratories. The consistent findings have established that BJ-Snt is a suitable standard for bracketing *in situ* S isotope measurement using LA-MC-ICP-MS, and the recommended $\delta^{34}S$ value determined by IRMS was $-0.71 \pm 0.32‰$ (2 s, $n = 15$).

Received 12th September 2023
Accepted 20th November 2023

DOI: 10.1039/d3ja00308f

rsc.li/jaas

1. Introduction

Antimony is a non-renewable strategic mineral resource and has been designated as a key metal of strategic importance by major countries such as China and the United States.[1–3] Stibnite is among the most important Sb-bearing mineral phases in the majority of Sb deposits and it even occur as the exclusive Sb-bearing ore mineral in some large Sb deposits.[4–7] Therefore, the geochemistry of stibnite, particularly the sulfur isotopic variations at a sub-grain scale, often harbors valuable information for elucidating the sources of sulfur in hydrothermal fluids and ore-forming processes of Sb deposits.[8,9]

Conventional techniques for obtaining sulfur isotope ratios mainly refer to solution nebulizer multi-collector inductively coupled plasma mass spectrometry (SN-MC-ICP-MS), multi-collector thermal ionization mass spectrometry (MC-TIMS) and gas-source mass spectrometry (GS-MS).[10,11,16–21] These methods possess an absolute advantage in achieving higher precision determination of sulfur isotope ratios (~0.1–0.25‰) compared to other measurements, such as SIMS and ICP-SF-MS. Meanwhile, their characteristics of bulk-rock analysis are destined with the drawback of complex and time-consuming sample preparation, as well as losing the spatial information.[12–15] In comparison, laser ablation multi-collector inductively coupled plasma mass spectrometry (LA-MC-ICP-MS) is more valued by geologists due to its superior spatial resolution at the micrometer scale. Additionally, it offers advantages such as low contamination, affordability, high efficiency, and minimal water-related spectral interference.[22,23] However, the applications of LA-MC-ICP-MS are significantly limited by matrix effects and fractionation effects arising from variations in the crater depth, signal intensity, aerosol size distribution, vaporization, and ionization of the ablated particles within ICP.[24] The accuracy and precision of the analysis are also compromised by isotopic fractionation and spectrum interference. Therefore, numerous efforts have been made to enhance the accuracy and precision of measurements, including simulating isotopic fractionation behavior, mitigating interfering substances, and developing matrix-matched reference materials.[25–30] Among them, the inclusion of a matrix-matched reference material is imperative to enhance

[a]State Key Laboratory of Ore Deposit Geochemistry, Institute of Geochemistry, Chinese Academy of Sciences, Guiyang 550081, China. E-mail: daizhihui@mail.gyig.ac.cn; fushanling@mail.gyig.ac.cn
[b]School of Chemistry and Environmental Engineering, Hanshan Normal University, Chaozhou 521041, China
[c]State Key Laboratory of Continental Dynamics, Department of Geology, Northwest University, Xi'an 710069, China
[d]Institute of Mineral Resources, Chinese Academy of Geological Sciences, Beijing 100037, China

the accuracy and precision of measurements pertaining to sulfur isotope ratios.

The current certified solid sulfide standards for sulfur isotopes include the IAEA series (Ag_2S powder) and NBS123 (ZnS). With the advancement of *in situ* microanalysis, natural minerals, compressed powder tablets, and artificial solid samples have been utilized as calibrated materials for S isotope analysis in a wide range of sulfide minerals, including pyrite, pentlandite, pyrrhotite, sphalerite, and chalcopyrite.[22,24,31–38] The noteworthy point is that IRMS is a more prevalent approach for determining S isotopes in stibnite, owing to its independence of matrix-matched reference materials.[39–41] The IAEA series has traditionally been employed as standard materials for *in situ* S isotope microanalysis.[42,43] For example, the sulfur isotope ratios in stibnite from the Xikuangshan Sb deposit were determined using LA-MC-ICP-MS with IAEA-S-1 as the calibrator and the in-house standard Cpy-1/GC as a quality control, as reported by Fu *et al.* (2020).[9] Other materials, such as sphalerite (NBS123), chalcopyrite (Cpy-1) and galena (CBI-3), were also utilized for S isotope analysis of stibnite.[44–46]

Notably, the presence of matrix effects would induce substantial instrumental mass bias, thereby compromising the accuracy and precision of measurements. For example,[22] Chen *et al.* (2017) proposed that the deviation of $\delta^{34}S$ was less than 0.3‰ resulting from Cu and Fe, but increased to 0.7‰ as a result of Zn when the solution contained an equal concentration of matrix elements and sulfur. Therefore, the availability of isotopically homogeneous and well-characterized mineral standards that are matrix-matched is crucial for accurately determining the sulfur ratio using LA-MC-ICP-MS. This study proposes using natural stibnite (BJ-Snt) as a potential standard reference material for determining S isotopes in stibnite through LA-MC-ICP-MS analysis. Extensive data indicate that BJ-Snt exhibits consistent chemical characteristics, including homogenous S isotope compositions, concise mineral phases, and simple element compositions.

2. Experimental methods

2.1 Sample description and preparation

2.1.1 Synthesizing a nanoparticulate pressed stibnite powder tablet. The pressed powder tablet of stibnite (YS14) was mixed with natural stibnite grains, which were collected from Chenzhou in Hunan Province and smashed with an agate mortar. For microanalysis, the particles were milled to the nanoscale using a planetary ball mill (PM 100, Retsch, Germany) at the State Key Laboratory of Ore Deposit Geochemistry (SKLODG), Institute of Geochemistry, Chinese Academy of Sciences. The wet milling technique was described in Bao *et al.* (2017).[31] Milli-Q water (18.2 MΩ cm) was blended by ball-milling in suspension. The total milling time for one sample was 90 min with an interval of 5 min of milling and 1 min of cooling. The powder-water suspension was dried on a hotplate overnight at 90 °C, and then milled for 10 min using an agate mortar. Approximately 0.75 g powder materials were pressed into tablets (11 mm in diameter) using a hydraulic press without a binder at 30 MPa.

2.1.2 Preparation of the stibnite material. The natural stibnite BJ-Snt was obtained from the Baiji Pb–Zn–Sb ore deposit located in Weixi County, western Yunnan Province, China. This deposit is a small-scale epithermal deposit situated in the middle part of the Sanjiang metallogenic belt and northern regions of the Lanping Basin.[47]

A total of twenty-nine fragments were micro-drilled from the surface of the stibnite hand specimen BJ-Snt for LA-MC-ICP-MS

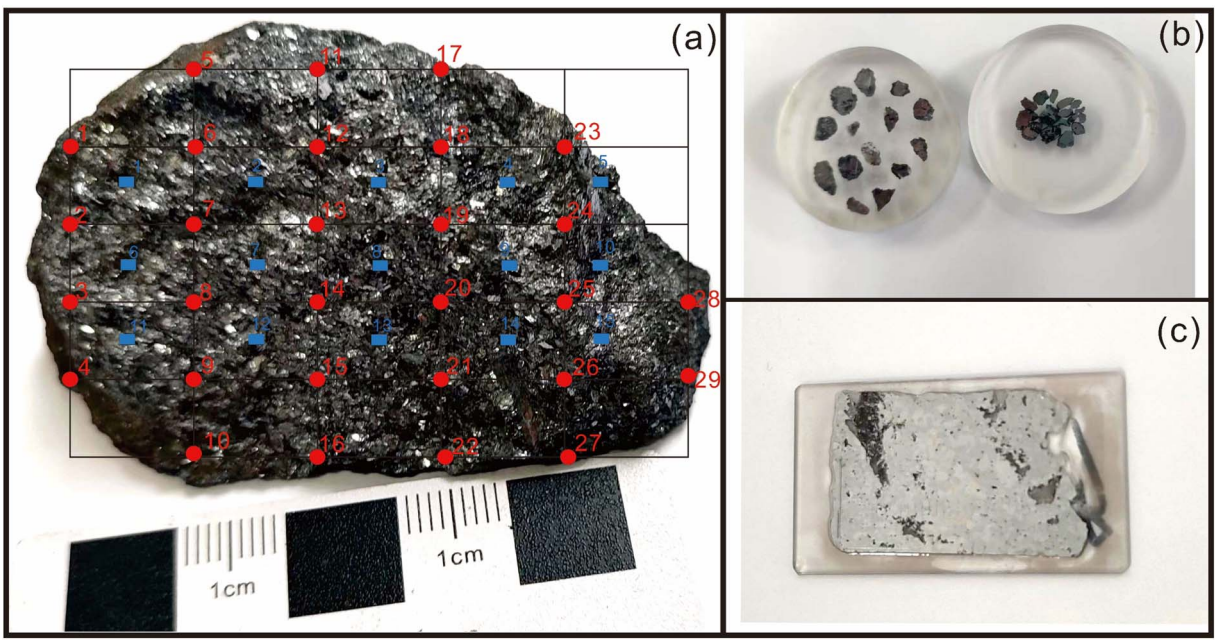

Fig. 1 The whole hand specimen of stibnite BJ-Snt investigated in this study. The red dot (a) shows 29 microdrilling positions on the stibnite specimen, and these fragments were fixed in two epoxy mounts (b). Blue box (a) labelled with 15 positions sampled for IRMS analysis. (c) Transection prepared from the BJ-Snt stibnite.

analysis. The micro-drilled positions were distributed on the nodes of the matrix, as depicted in Fig. 1a and b, with a vertical interval of 1 cm and a horizontal interval of 0.6 cm. Furthermore, a total of 15 positions were meticulously chosen for IRMS, ensuring an even distribution across the entire specimen (indicated by the blue boxes in Fig. 1a). Approximately 5 mg of powders from each position was promptly collected and immediately transferred to a clean sample bag. The sampling procedure employed a micro-drill with a diameter of 2.0 mm, specifically excluding the use of quartz and calcite. The drill bit was thoroughly cleansed using dust-free paper and anhydrous ethanol three times prior to drilling each position.

The entire sample was subsequently divided into two equal parts and then affixed onto a thin section (Fig. 1c). The epoxy mounts and the thin section were meticulously polished multiple times until achieving a flat and smooth surface devoid of any discernible scratches.

2.1.3 Other samples. Solid sulfur-bearing materials include an international sulfur reference material (NBS123) and natural samples (SZY, GC, and CDT-1). NBS123 is a sphalerite standard obtained from the National Institute of Standards and Technology (NIST). SZY consists of pure pyrite particles. GC is an in-house chalcopyrite reference material that was collected from the Guichi copper mine, Anhui, China.[36] CDT-1 is a fragment of Cañon Diablo troilite that originates from the vicinity of the Barringer Meteor Crater in Arizona, USA.[50] After being procured from meteorite dealers, the troilite samples were leached for 5 min in 0.05 M HCl in an attempt to remove surface contamination and embedded in epoxy resin. The practical values of S isotope ratios were determined by IRMS, with an average value of +0.17 ± 0.26‰ (Fig. 2).

2.2 Analytical techniques

2.2.1 Automated mineral quantitative analysis system. Mineral phases and SEM-based microscopy were analyzed using a TESCAN Integrated Mineral Analyser (TIMA). All analyses, were completed at SKLODG, Institute of Geochemistry, Chinese Academy of Sciences. The TIMA is an automated scanning electron microscopy system composed of TIMA hardware and version 1.5.50 TIMA software. Four energy-dispersive X-ray (EDX) detectors were attached to the large chamber of the VEGA (thermionic emission-tungsten) platform. High-resolution mapping mode was preferred with a 15 mm working distance with a 3 μm pixel size for our study. A 25 keV accelerating voltage, 4.76 nA probe current and 18.2 beam intensity were selected for a better mineral classification. The thin section was carbon-coated, and the total scan required approximately 14 hours with 1000 counts collected per analysis point.

2.2.2 Isotope ratio mass spectrometry. A total of 15 powdered samples of BJ-Snt were analysed using a gas isotope ratio mass spectrometer (MAT253) coupled to an elemental analyser (EA-IRMS, Flash EA 2000) to obtain the sulfur isotope compositions. Stibnite grains were hand-picked under a binocular microscope to ensure high purity and crushed to a 200 mesh. The trace powders (<100 μg) were injected into the reactor, which was filled with the reductant Cu and oxidizer WO_3. Sulfion would be converted to SO_2 at 1020 °C under a vacuum pressure of 2×10^{-2} Pa. An MAT253 mass spectrometer has the ability to accurately determine the product SO_2. Measurements were represented in standard δ-notation

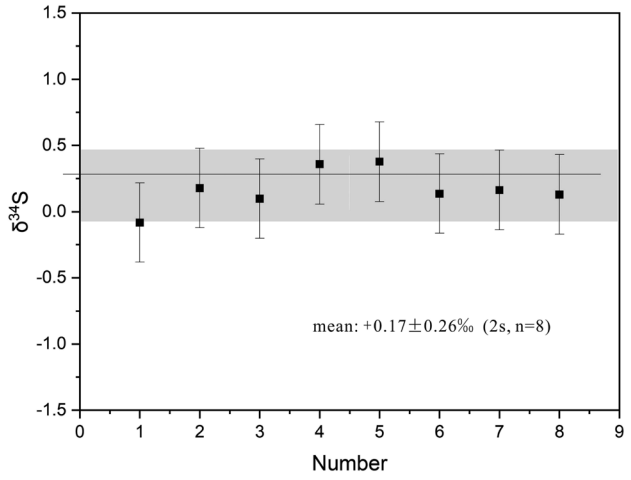

Fig. 2 $\delta^{34}S$ values of CDT-1 determined by IRMS. Error bars are determined by repeated measurements of IAEA reference materials as the unknowns.

Table 1 Instrument parameters for S isotope measurements and trace elements analyzed by LA-MC-ICP-MS and LA-ICP-MS

LA-ICP-MS at IGCAS		
ICP-MS	**Agilent 7700x**	
Forward power	1400	W
Carrier gas (Ar)	0.9	l min^{-1}
Oxide rate (Tho/Th)	<0.3	%
Doubly charged formation rate (Ca^{2+})	<0.3	%
Plasma condition (U/Th)	0.95–1.05	
Laser ablation	**Resolution-LR-S155**	
Wavelength	193	nm
Pulse length	5–10	ns
Energy density on the sample	2	J cm^{-2}
Pulse frequency	5	Hz
Spot size	26	μm
Carrier gas (He)	350	ml min^{-1}
LA-MC-ICP-MS at IGCAS		
MC-ICP-MS	**Nu plasma III**	
Forward power	1400	W
Carrier gas (Ar)	0.85	l min^{-1}
Integration time	0.4	s per cycle
Faraday cup configuration	H6–^{34}S; Ax–^{33}S; L5–^{32}S	
Mass resolution	Medium resolution	
Laser ablation	**Resolution-LR-S155**	
Wavelength	193	nm
Pulse length	5–10	ns
Energy density on the sample	2	J cm^{-2}
Pulse frequency	5	Hz
Spot size	60	μm
Carrier gas (He)	200	ml min^{-1}

relative to the VCDT international standard. The precision of $\delta^{34}S$ was better than 0.2‰ (1 s), as calculated from repeated analyses of IAEA-S-1 (−0.3‰), IAEA-S-2 (+22.62‰) and IAEA-S-3 (−32.49‰).

2.2.3 LA-ICP-MS. Quantitative mapping and concentration measurements of major and trace elements were conducted using an ASI RESOLution-LR-S155 laser microprobe equipped with a Coherent Compex-Pro 193 nm ArF excimer laser. An Agilent 7700x ICP-MS was used to acquire ion-signal intensities. The ablated aerosol was mixed with Ar (900 ml min^{-1}) and He (350 ml min^{-1}) in the ablated cell before exiting the cell. Detailed parameters are listed in Table 1. Quantitative analysis was run with a 26 μm pit size, 5 Hz pulse frequency and 2 J cm^{-2} fluence incorporating a background acquisition of approximately 30 s (gas blank) and 60 s of data acquisition. The parameters for mapping were 6 μm spot size, 10 Hz frequency and 2 J cm^{-2} fluence, matched with 10 μm s^{-1} scan speed. STDGL3 was used to determine the concentrations of chalcophile and siderophile elements.[49] The integrated count data to concentrations for lithophile elements were calibrated and converted using GSD-1G. Element concentrations were calculated by internal standardization (Sb) based on the normalization of the sum of all metal sulfides and oxides to 100 wt%.[52,53]

2.2.4 Laser ablation MC-ICP-MS. A MC-ICP-MS (Nu Plasma III, Nu Instruments, UK) coupled with a RESOlution-LR-S155 laser ablation system (ASI, Australia) was used for *in situ* sulfur isotope measurements. The laser ablation system consisted of a 193 nm ArF CompexPro102 excimer laser (Coherent, USA), a double-cell sample chamber, a computer-controller, and a high-precision X–Y sample positioning stage. The chamber had the advantage of avoiding cross-contamination and reducing the background flushing time. Helium (200 ml min^{-1}) was used as a carrier gas and mixed with argon (0.85 l min^{-1}) in the funnel cell. The sample aerosol was blended in the above-mentioned gas and transferred into the ICP immediately. The total acquisition time for single-spot ablation was 70 s with the following parameters: 10 s baseline time, 40 s ablation time, 20 s wash time, 60 μm spot size, 5 Hz repetition rate and 2 J cm^{-2} energy density. H6, Ax and L5 Faraday cups were used to collect ^{34}S, ^{33}S and ^{32}S, respectively. The instrument was operated in medium-resolution mode (resolution power = 3200)[51] to resolve polyatomic interference from ^{16}O–$^{16}O/^{15}N$–^{16}O–^{1}H for ^{32}S and ^{16}O–$^{18}O/^{17}O$–^{16}O–$^{1}H/^{33}S$–^{1}H for ^{34}S. During the analysis of the *in situ* S isotope, time-resolved mode was adopted with a minimum signal intensity of 5 V for ^{32}S. Detailed parameters are listed in Table 1.

The pressed powder tablet YS14 was employed to correct instrumental drift and mass bias for S isotope analysis by LA-MC-ICP-MS. The reasons mainly relied on: (1) some studies suggested that pressed powder tablets were perfect as bracketing calibrators;[31] (2) the S isotope compositions of YS14 were homogeneous, as determined by IRMS. All of the data were reported relative to $(^{34}S/^{32}S)_{V\text{-}CDT}$. The measured $^{34}S/^{32}S$ ratios were convenient to convert as a per mil (‰) variation relative to VCDT:

$$\delta^{34}S_{VCDT}\ (‰) = \frac{(^{34}S/^{32}S_{sam} - {}^{34}S/^{32}S_{std})}{(^{34}S/^{32}S_{std})} \times 1000$$

where sam and std are the measured sample and calibrated standard, respectively. $\delta^{34}S_{YS14}$ was converted to VCDT ($\delta^{34}S_{YS14} = -2.66 \pm 0.20‰$, 2 s, $n = 5$).

3. Results

3.1 Mineral analysis

The principal metallic minerals found in the ore bodies of the Baiji deposit include stibnite, zinkenite, sphalerite, and tetrahedrite. Additionally, there are minor occurrences of galena and cinnabar. The gangue minerals present are primarily calcite with minor amounts of quartz and siderite.[47] The BJ-Snt sample is predominantly composed of stibnite (87.59%), with minor occurrences of quartz (6.91%), calcite (4.13%), kaolinite (0.61%), pyrite (0.24%), and albite (0.15%) as revealed by the Panoramic BSE and TIMA mineral phases map in Fig. 3. The consistency was demonstrated based on the BSE maps and S distributions observed in the thin section (Fig. 4). The subsequent step involved the random selection of a stibnite particle for quantitative analysis, specifically focusing on mapping and element concentrations (Table 2 and Fig. 5). The results demonstrated that the sample solely consisted of consistent major elements (Sb ranging from 71.20 to 71.53 wt% and S ranging from 28.1 to 28.24 wt%) and hundreds to thousands

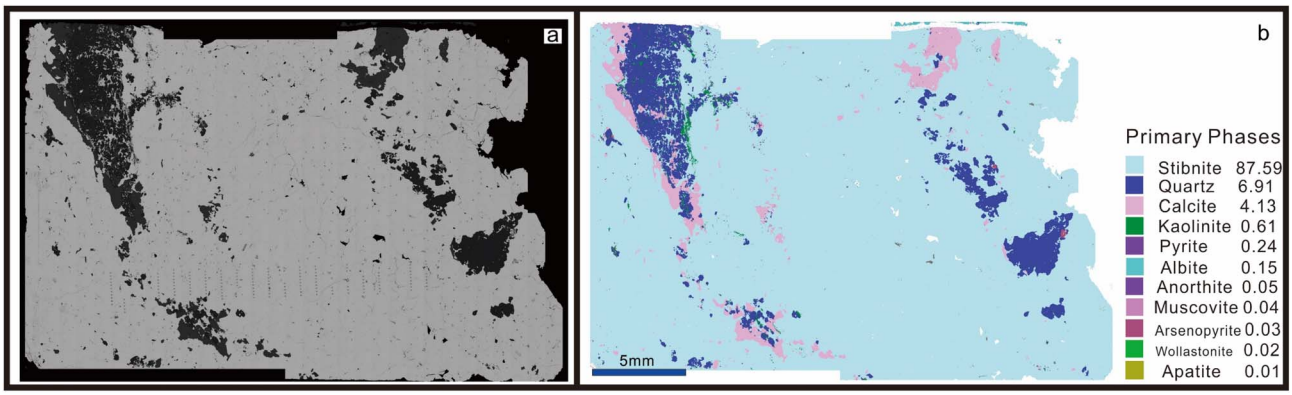

Fig. 3 Panoramic BSE (a) and TIMA mineral phase map (b) of the thin section.

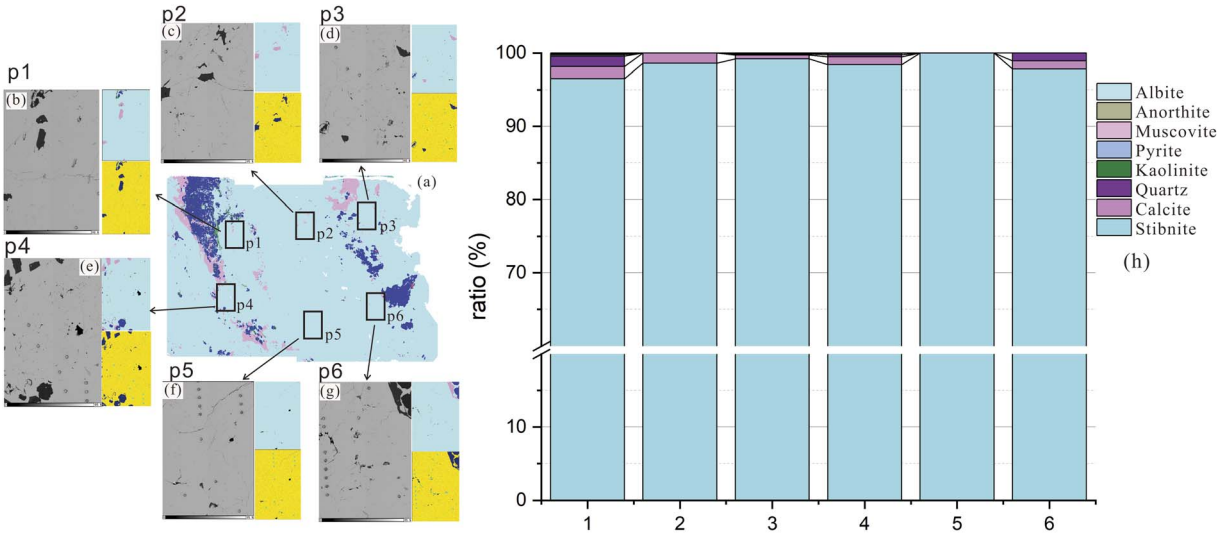

Fig. 4 Backscattered electron images and TIMA mineral phases maps and S distributions in different parts of the thin section. (a) TIMA maps. (b)–(g) Left pictures were the BSE images, top right were mineral phases, and bottom right were S distributions in different areas. (h) The composition of mineral phases in the above areas.

of ppm for trace elements (Si, Cu, As, and Pb). The difference in optical properties observed in the microscope can potentially be attributed to the presence of Cu and Pb. As a result, the BJ-Snt stibnite exhibits relatively homogeneous chemical compositions.

Table 2 Element concentrations of the stibnite BJ-Snt analysed by LA-ICP-MS

Sample	S (wt%)	Sb (wt%)	Si (ppm)	Cu (ppm)	As (ppm)	Pb (ppm)
BJ-1	28.18	71.35	908.08	364.33	701.44	1615.82
BJ-2	28.14	71.23	1276.73	407.72	685.32	1559.24
BJ-3	28.16	71.32	957.84	449.23	989.97	1649.44
BJ-4	28.16	71.31	930.55	447.67	975.80	1786.04
BJ-5	28.24	71.49	—	392.23	690.27	1645.97
BJ-6	28.19	71.39	940.83	298.01	703.07	1216.53
BJ-7	28.17	71.35	698.74	279.30	735.82	1116.50
BJ-8	28.24	71.53	—	327.57	751.62	1163.64
BJ-9	28.21	71.46	—	444.96	1210.78	1592.28
BJ-10	28.14	71.29	1176.94	396.95	1177.87	1613.62
BJ-11	28.20	71.40	418.51	266.11	871.18	1881.84
BJ-12	28.23	71.48	—	398.71	932.55	1614.91
BJ-13	28.19	71.39	861.18	304.53	732.09	1263.63
BJ-14	28.19	71.38	921.39	338.69	685.50	1280.07
BJ-15	28.20	71.39	636.97	394.22	809.29	1541.74
BJ-16	28.19	71.39	717.63	341.09	773.37	1540.37
BJ-17	28.21	71.48	—	240.58	1062.64	1464.38
BJ-18	28.19	71.38	676.48	423.69	852.40	1581.89
BJ-20	28.19	71.38	721.49	423.49	821.79	1538.62
BJ-21	28.13	71.26	654.61	272.31	873.40	1336.53
BJ-22	28.14	71.27	647.86	190.66	664.36	1371.25
BJ-23	28.12	71.23	654.91	312.83	944.56	1332.43
BJ-24	28.11	71.21	669.52	371.88	1195.05	1354.94
BJ-25	28.13	71.24	671.49	298.98	690.65	1286.70
BJ-26	28.12	71.21	725.58	380.00	886.34	1420.73
BJ-27	28.13	71.24	672.32	356.15	827.80	1370.93
BJ-28	28.12	71.20	714.26	409.03	955.00	1576.76
BJ-29	28.14	71.26	629.53	363.12	791.93	1392.07
BJ-30	28.13	71.25	640.45	375.80	853.09	1364.71
BJ-31	28.14	71.24	649.50	419.97	747.25	1525.58

3.2 IRMS measurement

Fifteen stibnite fragments of BJ-Snt were selected and analyzed by IRMS. $\delta^{34}S$ values ranged from −1.00‰ to −0.46‰ with a mean of −0.71 ± 0.32‰ (2 s, $n = 15$). The measured data are given in Fig. 6. The S isotope ratios of IAEA-S-2 and IAEA-S-3 were +22.3 ± 0.24‰ (2 s, $n = 8$) and −32.3 ± 0.24‰ (2 s, $n = 8$), respectively, which align perfectly with the published values. The credibility of the value determined by IRMS was ensured when it exhibited consistent S isotope compositions.

3.3 LA-MC-ICP-MS measurement results

A total of 505 $\delta^{34}S$ spot values were obtained using LA-MC-ICP-MS on two epoxy mounts and a thin section to investigate the isotopic homogeneity of S in BJ-Snt (Fig. 7). Among them, 207 and 182 spots were acquired in mount1 and mount2, which yield $\delta^{34}S$ values ranging from −1.34‰ to −0.46‰ and −1.36‰ to −0.35‰, with average values of −0.82 ± 0.32‰ and −0.73 ± 0.39‰, respectively (2 s, Fig. 7a and b). Mineral phases would undergo filtration prior to laser ablation. In the thin section, the mean $\delta^{34}S$ was −0.79 ± 0.28‰, which was determined from 116 measurements ranging from −1.13‰ to −0.53‰ (Fig. 7c). The values of the dataset followed a Gaussian distribution, resulting in an average value of −0.78 ± 0.34‰ (2 s, $n = 505$, Fig. 7d–f). This average value was found to be consistent with the values obtained through IRMS (−0.71 ± 0.32‰) within a 2 s analytical uncertainty. Furthermore, the result also demonstrated that the difference resulting from physical characteristics between powder pressed pellets and natural crystals can be ignored, consisted with Chen *et al.* (2017).[22] It means that the in-house stibnite material (YS14) is viable as the bracketing calibrator based on the homogenous S isotope compositions.

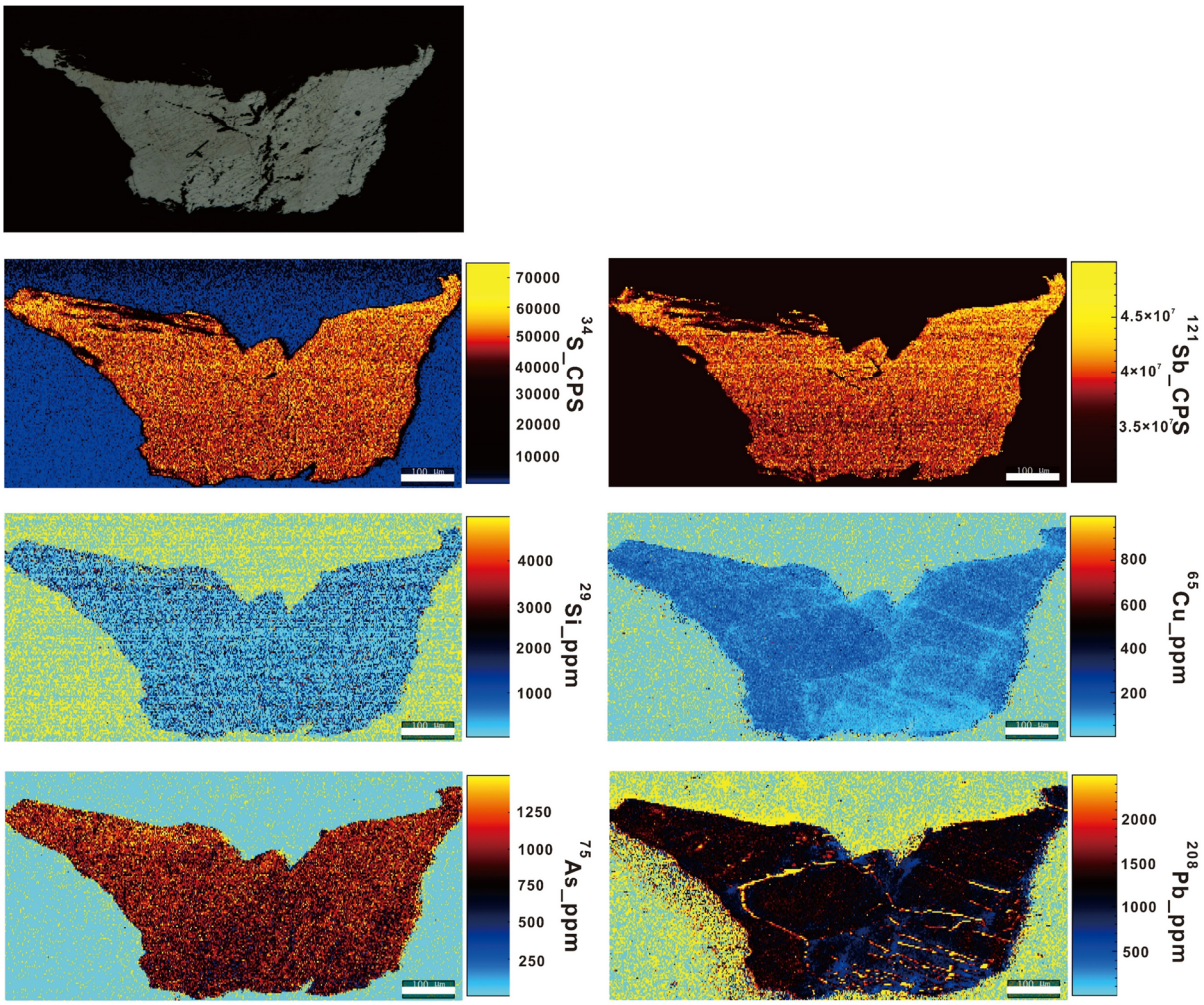

Fig. 5 Element distributions in a fragment of the stibnite BJ-Snt.

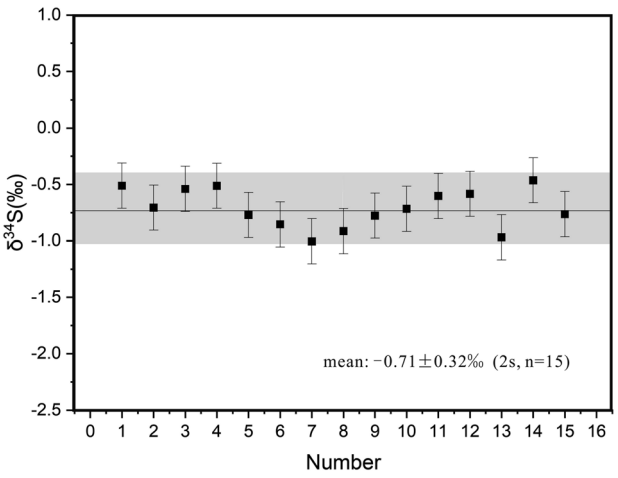

Fig. 6 $\delta^{34}S$ values of BJ-Snt stibnite determined by IRMS. Error bars are determined by repeated measurements of IAEA reference materials as the unknowns.

3.4 Differences caused by different matrices

The differences in sulfur isotope microanalysis between the standard and sample may be attributed to variations in the sulfur concentration, chemical composition, and physical structure.[22] In this study, the disparities in stibnite sulfur isotopic analysis were assessed through comparisons of various calibration materials, including stibnite (YS14), sphalerite (NBS123), chalcopyrite (GC), pyrite (SZY) and troilite (CDT-1). All adopted standard materials were natural crystals (except for YS14) to exclude the interference of the physical structure. The calibrated object was the S isotope compositions of BJ-Snt, which are listed in Fig. 8 and Table 3. Calibrated using the standard materials YS14, NBS123, GC, and CDT-1 with approximate S concentrations, the mean $\delta^{34}S$ values obtained for BJ-Snt were $-0.72 \pm 0.22‰$ (2 s, $n = 80$), $-0.55 \pm 0.26‰$ (2 s, $n = 80$), $+0.09 \pm 0.26‰$ (2 s, $n = 80$), and $+0.76 \pm 0.34‰$ (2 s, $n = 40$). Notably, the S isotope ratios were approximately 1.40‰ higher when CDT-1 was used as the calibrator. Comparably, NBS123 can be considered as a secondary option for calibrating the S isotopes of stibnite. Additionally, approximate $\delta^{34}S$ values

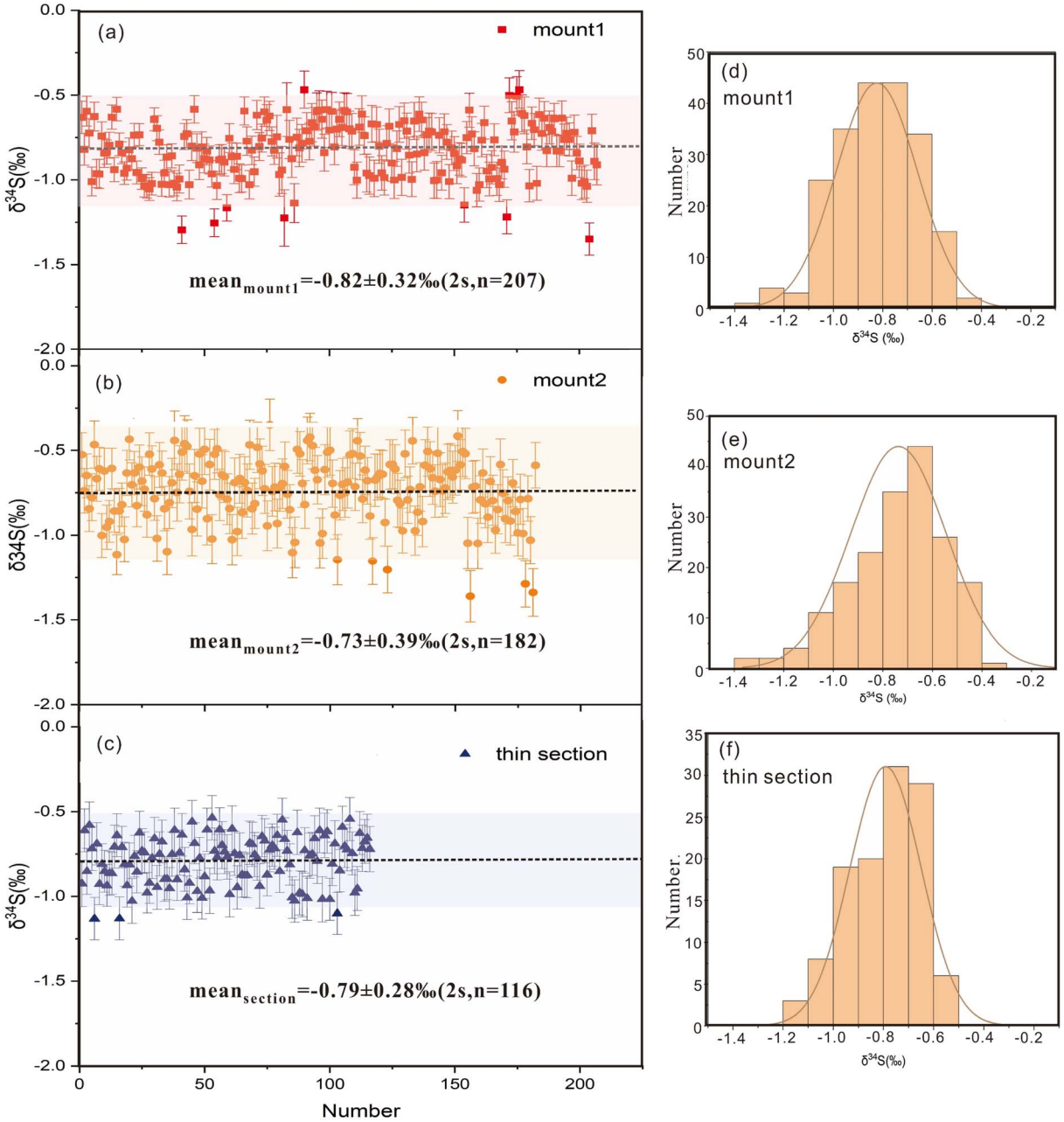

Fig. 7 Statistics of $\delta^{34}S$ values for two epoxy mounts and a thin section. (a)–(c) $\delta^{34}S$ values determined by LA-MC-ICP-MS. Range bars represent internal precision (2 s) and the gray area shows the external precision of multiple tests (2 s); (d)–(f) frequency histograms and probability density curves.

were obtained when using SZY and CDT-1 as bracketing calibrators, which corresponded to distinct S contents (53.45 wt% of SZY and 34.47 wt% of CDT-1). As such, the S concentration is evidently not a determining factor for assessing the suitability of the bracketing calibrator. In contrast, the chemical composition is the primary factor that can potentially influence variations in the ablated mass, aerosol size distribution, vaporization, and ionization regions of particles within the ICP. Therefore, it is essential to employ matrix matching materials when conducting S isotope microanalysis of stibnite.

3.5 Reproducibility of $\delta^{34}S$ values

The standard deviation (SD) was commonly employed to quantify the variability of $\delta^{34}S$ values. The data acquired in two mounts and a thin section were mathematically summarized, yielding a double-SD of 0.32‰, 0.39‰ and 0.28‰, respectively. These findings indicate a high level of homogeneity in S isotope compositions for the entire sample of stibnite BJ-Snt (Fig. 7). In addition, even when calibrated using different standard materials (Fig. 8), the precision remained excellent, ranging from 0.26‰ to 0.34‰.

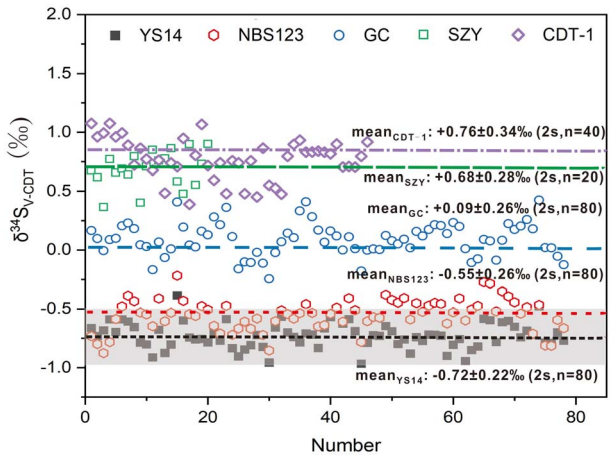

Fig. 8 $\delta^{34}S$ values of BJ-Snt using YS14, NBS123, GC, SZY and CDT-1 as bracketing standards. The gray area indicates the external precision (2 s) calculated using the stibnite powder pressed pellets (YS14). Dotted lines represent the averaged values of each set of data.

Intercomparison among participating laboratories is essential to validate the accuracy of our findings. Two stibnite grains were randomly selected and independently analysed at two laboratories. The obtained $\delta^{34}S$ values of BJ-Snt were $-0.78 \pm 0.14‰$ (2 s, $n = 18$, LA-MC-ICP-MS, Nanjing FocuMS Technology Co. Ltd, China) and $-0.90 \pm 0.16‰$ (2 s, $n = 19$, LA-MC-ICP-MS, State Key Laboratory of Continental Dynamics, Department of Geology, Northwest University), resulting in an optimistic outcome. The external precision (0.14 to 0.16‰) demonstrates the homogeneity of S isotope compositions in the stibnite BJ-Snt, thereby confirming its suitability as a standard calibrator for S isotope analysis using LA-MC-ICP-MS.

4. Applications

Primary utilization of the stibnite BJ-Snt was conducted in this study. The stibnite crystal, with dimensions of approximately 200 mm length, 150 mm width, and 50 mm height, was extracted from the sample ZZX-1 within the Zhazixi Sb-W deposit located in the central part of the Xuefeng uplift in South China. Antimony orebodies of the Zhazixi deposit are primarily hosted in the tuffaceous slate and tuffaceous sandstone, characterized by a simple mineral assemblage primarily composed of stibnite and quartz, with trace amounts of arsenopyrite. The principal sulfide in the orebodies of the Zhazixi deposit is stibnite, with negligible amounts of other sulfides and sulfates. Therefore, the $\delta^{34}S$ values of stibnite can accurately represent the total sulfur content in the ore fluids of this deposit.

A random cross section was split and fixed in a thin section for *in situ* analysis of LA-MC-ICP-MS, and 19 fragments were

Table 3 $\delta^{34}S$ values of BJ-Snt using different matrices as standard calibrators and theoretical information of minerals

		Composition (wt%)						
Mineral	Chemical formula	S	Sb	Zn	Fe	Cu	Cell dimensions	$\delta^{34}S_{V-CDT}$ (‰)
Stibnite (YS14)	Sb_2S_3	28.32	71.68				$a = 11.229$ nm, $b = 11.31$ nm, $c = 3.893$ nm, $Z = 4$	-0.72 ± 0.22
Sphalerite (NBS123)	(Zn,Fe)S	33.06		64.06	2.88		$a = 5.406$ nm, $Z = 4$	-0.55 ± 0.26
Chalcopyrite (GC)	$CuFeS_2$	34.94			30.43	34.63	$a = 5.28$ nm, $c = 10.41$ nm, $Z = 4$	$+0.09 \pm 0.26$
Pyrite (SZY)	FeS_2	53.45			46.55		$a = 5.417$ nm, $Z = 4$	$+0.68 \pm 0.28$
Troilite (CDT-1)	FeS	34.47			63.53		$a = 3.452$ nm, $c = 5.762$ nm, $Z = 2$	$+0.76 \pm 0.34$

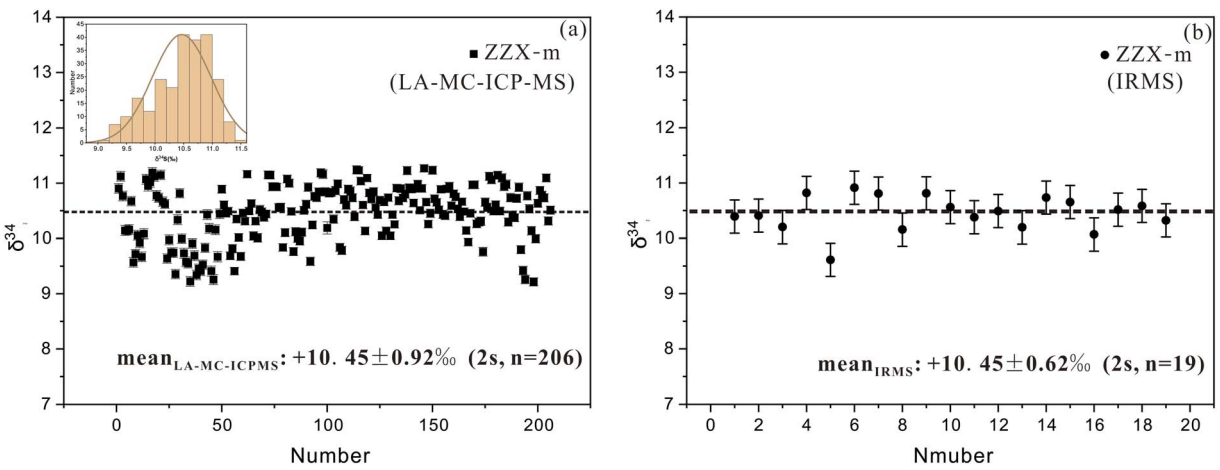

Fig. 9 Comparison of $\delta^{34}S$ values of the stibnite ZZX-m analysed by LA-MC-ICP-MS and IRMS: (a) statistics of $\delta^{34}S$ (‰) obtained by LA-MC-ICP-MS in the thin section. Inset: frequency histograms and probability density curves. (b) $\delta^{34}S$ values based on IRMS for different fragments.

selected for the analysis by IRMS. BJ-Snt was applied as a bracketing calibrator for the $\delta^{34}S$ ratios, matched with the SSB method. The $\delta^{34}S$ results analysed in the thin section suggest that the $\delta^{34}S$ values were concentrated in a narrow range (+9.22‰ to +11.16‰, Fig. 9a), following a Gaussian distribution with a mean value of +10.45 ± 0.92‰ (2 s, n = 206, Fig. 9c). These values are highly consistent with the approximate value (+10.45 ± 0.62‰, 2 s, n = 19) obtained by IRMS (Fig. 9b). The homogeneous and high $\delta^{34}S$ values indicate that the sulfur in ore fluids may have exclusively been derived from a common origin (*e.g.*, neoproterozoic basement) without significant involvement of magmatic sulfur.[9,48]

We discovered that $\delta^{34}S$ values were also consistent on a small scale in the thin section of ZZX-m. To confirm the appearance, the whole specimen was crushed into dozens of fragments, in which 13 fragments were selected randomly for LA-MC-ICP-MS. Calibrated by BJ-Snt, a total of 390 $\delta^{34}S$ values in 13 fragments were obtained (Table 4). The standard deviation (SD) concurrently with the mean can be used to accurately estimate the variation in normally distributed data. The range of two standard deviations from the mean is expected to encompass approximately 95% of the observed individuals. Herein the two SDs of $\delta^{34}S$ values in 13 fragments are concentrated in the narrow range of 0.33 to 0.49‰, suggesting that the S isotope ratios were also homogeneous in a single crystal. The average value of +10.6‰ was the central tendency for the 13 fragments, which agrees well with that in the thin section. In addition, a few fragments were centered at + 9.8‰ and + 10.2‰. The consistent S isotope composition in the single crystal of the sample ZZX-m makes it a promising reference material that might be employed for quality control and method validation for LA-MC-ICP-MS.

The method validity of BJ-Snt was confirmed by conducting interlaboratory comparisons on three randomly selected stibnite fragments from ZZX-m. The $\delta^{34}S$ values of the samples were initially determined in our laboratory using BJ-Snt as a standard calibrator. Subsequently, the $\delta^{34}S$ values were independently measured at three other laboratories using YS14 for calibrations ((1) Nanjing FocuMS Technology Co. Ltd, China, (2) State Key Laboratory of Continental Dynamics, Department of Geology, Northwest University, and (3) Institute of Mineral Resources, Chinese Academy of Geological Sciences). The results of different laboratory analyses using YS14 and BJ-Snt as calibrators are listed in Fig. 10 and Table 5. The highly consistent results of the analysis further clarify that BJ-Snt is a suitable standard reference material for *in situ* S isotope measurement of LA-MC-ICP-MS.

Table 4 Information on $\delta^{34}S$ values (‰) for the 13 fragments of ZZX-m analysed by LA-MC-ICP-MS

	Average value	2 SDs	Number	Range
Fragment1	9.98	0.33	30	9.59–10.31
Fragment2	10.35	0.39	30	10.12–10.81
Fragment3	10.63	0.33	30	10.21–10.88
Fragment4	10.69	0.47	30	10.01–10.99
Fragment5	10.70	0.35	30	10.22–10.95
Fragment6	9.73	0.41	30	9.44–10.15
Fragment7	10.25	0.40	30	9.82–10.58
Fragment8	9.72	0.39	30	9.36–10.08
Fragment9	10.56	0.47	30	10.20–10.96
Fragment10	10.97	0.37	30	10.44–11.25
Fragment11	10.64	0.33	30	10.32–10.97
Fragment12	10.52	0.42	30	10.15–11.00
Fragment13	9.84	0.49	30	9.36–0.07

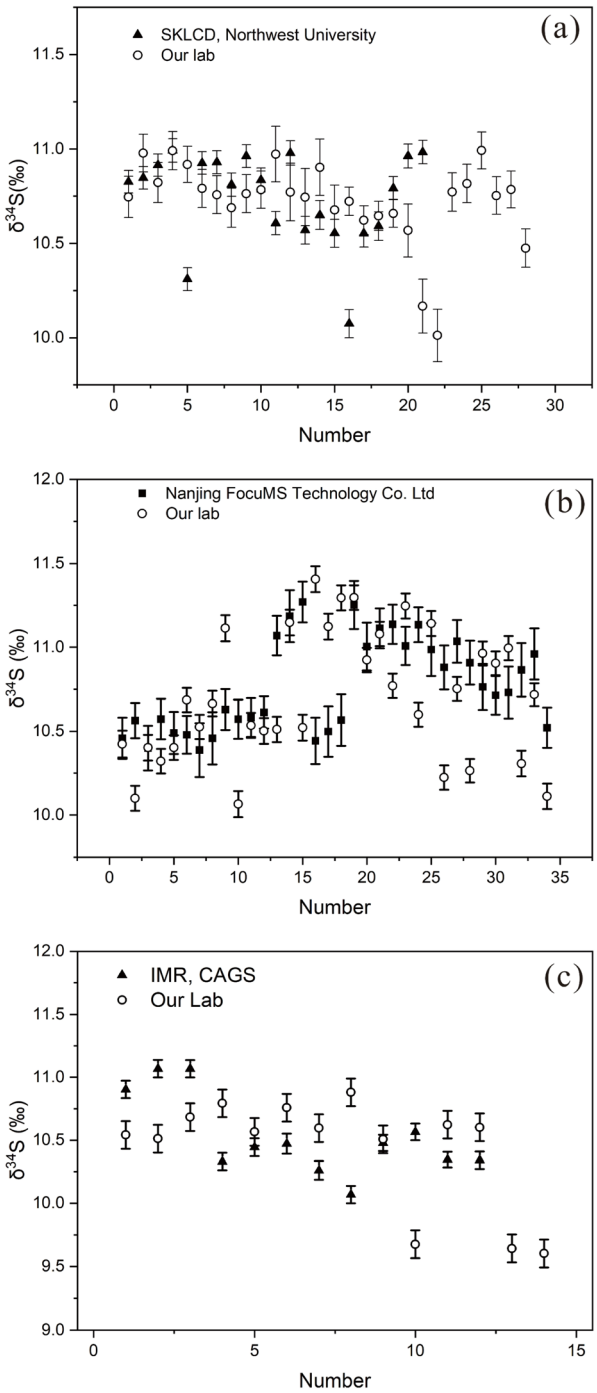

Fig. 10 Intercomparison of $\delta^{34}S$ values calibrated with YS14 and BJ-Snt in different laboratories for three fragments. (a)–(c) Three stibnite fragments.

Table 5 Summary of the δ34S values for three fragments of ZZX-m

		Means (‰)	2 SDs (‰)	*n*	Instrument	Calibrator
Fragment1	SKLCD, Northwest University	10.75	0.48	21	Nu 1700 + CompexPro 102	YS14
	Our lab	10.72	0.43	28	Nu plasma Ⅲ+ resolution-LR	BJ-Snt
Fragment2	Nanjing, FoucuMS	10.77	0.55	34	Nu plasma II + resolution-LR	YS14
	Our lab	10.71	0.76	34	Nu plasma Ⅲ + resolution-LR	BJ-Snt
Fragment3	Institute of mineral resources, CAGS	10.52	0.60	12	Finnigan Neptune + resolution-LR	YS14
	Our lab	10.42	0.67	14	Nu plasma Ⅲ + resolution-LR	BJ-Snt

5. Conclusions

The BJ-Snt hand specimen investigated in this study is composed of concise mineral phases and simple element compositions. A large amount of data demonstrated that the BJ-Snt grain has relatively homogeneous S isotope compositions determined by IRMS and LA-MC-ICP-MS. Hence, the stibnite BJ-Snt is a suitable natural reference material for *in situ* S isotope measurements of stibnite by LA-MC-ICP-MS. $-0.71 \pm 0.32‰$ (2 s, $n = 15$) determined by IRMS is the recommended $\delta^{34}S$ value for the BJ-Snt stibnite.

Author contributions

Zhihui Dai and Shanling Fu: conceptualization, methodology, formal analysis, data curation, writing – original draft, writing-review & editing, and funding acquisition; Yuefu Liu and Yumiao Meng: resources, sample collection and writing-review & editing. Zhian Bao and Kejun Hou: methodology, data curation and writing-review & editing; Tingguang Lan: methodology, supervision, and writing-review & editing.

Conflicts of interest

The authors declare that they have no known competing financial interests or personal relationships that could have appeared to influence the work reported in this paper.

Acknowledgements

We thank Dr Liang Li for the LA-MC-ICP-MS analysis, Dr Jing Gu for the IRMS analysis, and Chao Wang for the TIMA analysis. This study was financially supported by the projects of the National Key Research and Development Program of China (2023YFC2906801), Natural Science Foundation of China (42273083 and 42077313), Guizhou Provincial 2020 Science and Technology Subsidies (No. GZ2020SIG) and Special Fund of the State Key Laboratory of Ore Deposit Geochemistry (202303).

References

1 J. Ding, Y. Yang and F. Deng, *Geol. China*, 2013, **40**, 846–858.
2 J. Ding, Y. Zhang, Y. Ma, Y. Wang, J. Zhang and T. Zhang, *J. Geochem. Explor.*, 2021, **230**, 1–22.
3 Y. Wang, Y. Chen, D. Wang, J. Xu, Z. Chen and T. Liang, *Geol. China*, 2013, **40**, 1366–1378.
4 A. E. WilliamsJones and C. Normand, *Econ. Geol. Bull. Soc. Econ. Geol.*, 1997, **92**, 308–324.
5 A. Kyono, A. Hayakawa and M. Horiki, *Phys. Chem. Miner.*, 2015, **42**, 475–490.
6 H. G. Dill, *J. South Am. Earth Sci.*, 2003, **16**, 301–320.
7 J. T. Peng, R. Z. Hu, J. H. Zhao and Y. Z. Fu, *Bull. Mineral., Petrol. Geochem.*, 2003, **22**, 193–196.
8 P. R. Craddock, O. J. Rouxel, L. A. Ball and W. Bach, *Chem. Geol.*, 2008, **253**, 102–113.
9 S. L. Fu, R. Z. Hu, R. S. Yin, J. Yan, X. F. Mi, Z. C. Song and N. A. Sullivan, *Miner. Deposita*, 2020, **55**, 1353–1364.
10 M. Yun, M. A. Wadleigh and A. Pye, *Chem. Geol.*, 2004, **204**, 369–376.
11 A. Studley, E. M. Ripley, E. R. Elswick, M. J. Dorais, J. Fong, D. Finkelstein and L. M. Pratt, *Chem. Geol.*, 2002, **192**, 141–148.
12 G. Thode, J. Monster and H. B. Dunford, *Geochim. Cosmochim. Acta*, 1961, **25**, 159–174.
13 P. Fritz, R. J. Drimmie and V. K. Nowicki, *Anal. Chem.*, 1974, **46**, 164–166.
14 B. W. Robinson and M. Kusakabe, *Anal. Chem.*, 1975, **47**, 1179–1181.
15 H. P. Qi and T. B. Coplen, *Chem. Geol.*, 2003, **199**, 183–187.
16 A. Imai, N. Shikazono, M. Shimizu and H. Shimazaki, *Resour. Geol.*, 2006, **56**, 37–48.
17 Z. Y. Long, K. F. Qiu, M. Santosh, H. C. Yu, X. Y. Jiang, L. Q. Zou and D. W. Tang, *Geol. Soc. Am. Bull.*, 2023, **135**, 286–294.
18 J. L. Mann and W. R. Kelly, *Rapid Commun. Mass Spectrom.*, 2005, **19**, 3429–3441.
19 R. Clough, P. Evans, T. Catterick and E. H. Evans, *Anal. Chem.*, 2006, **78**, 6126–6132.
20 F. Albarede and B. Beard, *Geochemistry of Non-Traditional Stable Isotopes*, ed. C. M. Johnson, B. L. Beard and F. Albarede, 2004, pp. 113–152.
21 A. D. Anbar and O. Rouxel, *Annu. Rev. Earth Planet. Sci.*, 2007, **35**, 717–746.
22 L. Chen, K. Y. Chen, Z. A. Bao, P. Liang, T. T. Sun and H. L. Yuan, *J. Anal. At. Spectrom.*, 2017, **32**, 107–116.
23 Y. Fang, H. M. Yu, L. W. Xie, S. B. Fang, F. Huang and W. Y. Li, *J. Anal. At. Spectrom.*, 2023, **38**, 1626–1633.
24 Z. A. Bao, K. Y. Chen, C. L. Zong and H. L. Yuan, *J. Anal. At. Spectrom.*, 2021, **36**, 1657–1665.

25 W. Zhang and Z. C. Hu, *Spectrochim. Acta, Part B*, 2020, **171**, 1–15.
26 Z. Y. Zhu, S. Y. Jiang, C. L. Ciobanu, T. Yang and N. J. Cook, *Chem. Geol.*, 2017, **450**, 223–234.
27 D. S. Yang, M. Shimizu, H. Shimazaki, X. H. Li and Q. L. Xie, *Resour. Geol.*, 2006, **56**, 385–396.
28 T. Ushikubo, K. H. Williford, J. Farquhar, D. T. Johnston, M. J. Van Kranendonk and J. W. Valley, *Chem. Geol.*, 2014, **383**, 86–99.
29 M. J. Pribil, W. I. Ridley and P. Emsbo, *Chem. Geol.*, 2015, **412**, 99–106.
30 J. Mikova, J. Kosler and M. Wiedenbeck, *J. Anal. At. Spectrom.*, 2014, **29**, 903–914.
31 Z. A. Bao, L. Chen, C. L. Zong, H. L. Yuan, K. Y. Chen and M. N. Dai, *Int. J. Mass Spectrom.*, 2017, **421**, 255–262.
32 K. Y. Chen, Z. A. Bao, P. Liang, X. Nie, C. L. Zong and H. L. Yuan, *Spectrochim. Acta, Part B*, 2022, **188**, 1–10.
33 L. Chen, Y. Liu, Y. Li, Q. L. Li and X. H. Li, *J. Anal. At. Spectrom.*, 2021, **36**, 1431–1440.
34 Y. T. Feng, W. Zhang, Z. C. Hu, T. Luo, M. Li, Y. S. Liu, H. Liu and Q. L. Li, *J. Anal. At. Spectrom.*, 2022, **37**, 551–562.
35 R. C. Li, X. P. Xia, H. Y. Chen, N. P. Wu, T. P. Zhao, C. Lai, Q. Yang and Y. Q. Zhang, *Geostand. Geoanal. Res.*, 2020, **44**, 485–500.
36 N. Lv, Z. A. Bao, K. Y. Chen, C. L. Zong, Y. Zhang and H. L. Yuan, *Geostand. Geoanal. Res.*, 2022, **46**, 451–463.
37 X. Nie, Z. A. Bao, C. L. Zong, N. Lv, K. Y. Chen and H. L. Yuan, *J. Anal. At. Spectrom.*, 2023, **38**, 1065–1075.
38 Z. K. Zhou, H. Li, Y. Kotaro, A. Imai and T. Tindell, *J. Geochem. Explor.*, 2023, **247**, 107–177.
39 J. Chen, R. D. Yang, J. B. Gao, L. L. Zheng, L. J. Du, M. G. Yuan and H. R. Wei, *Acta Geochim.*, 2017, **36**, 339–352.
40 A. Zhaanbaeva, K. Peng, A. Oyebamiji and K. Asilbekov, *Acta Geochim.*, 2021, **40**, 659–675.
41 Z. Y. Song, Y. C. Yang, S. J. Han, B. Y. Li, Z. J. Zeng and T. W. Chen, *J. Geochem. Explor.*, 2023, **249**, 107–217.
42 S. L. Fu, T. X. Wang, J. Yan, L. C. Pan, L. M. Wei, Q. Lan and S. Y. Fu, *Ore Geol. Rev.*, 2022, **146**, 104949.
43 X. F. Song, J. Q. Lai, J. W. Xu, X. H. Liu, B. Li, H. S. He, Y. H. Wang, J. Shi, C. Wang and C. Wen, *J. Geochem. Explor.*, 2022, **12**, 1407.
44 J. Chen, Z. L. Huang, R. D. Yang, L. J. Du and M. Y. Liao, *Geosci. Front.*, 2021, **12**, 605–623.
45 J. Chen, X. R. Ni, L. J. Du, J. B. Gao, Z. F. Yang, L. L. Liu, Y. B. Ji and R. D. Yang, *Ore Geol. Rev.*, 2023, **156**, 105397.
46 Z. Y. Zhang, G. Q. Xie and P. Olin, *Ore Geol. Rev.*, 2022, **143**, 104781.
47 Y. F. Liu, H. W. Qi, X. W. Bi, R. Z. Hu, L. K. Qi, R. S. Yin and Y. Y. Tang, *Ore Geol. Rev.*, 2021, **131**, 104016.
48 G. P. Zeng, Y. J. Gong, Z. F. Wang, X. L. Hu and S. F. Xiong, *J. Geochem. Explor.*, 2017, **182**, 10–21.
49 L. Danyushevsky, P. Robinson, G. Sarah, M. Norman, L. Ross, P. McGoldrick and S. Michael, *Geochem.: Explor., Environ., Anal.*, 2011, **11**, 51–60.
50 C. E. McEwing, C. E. Rees and H. G. Thode, *Meteoritics*, 1983, **3**, 171–178.
51 M. A. Millet, J. A. Baker and C. E. Payne, *J. Geochem. Explor.*, 2017, **182**, 10–21.
52 Y. S. Liu, Z. C. Hu, S. Gao, D. Guenther, J. Xu, C. G. Gao and H. H. Chen, *Chem. Geol.*, 2008, **257**, 34–43.
53 M. H. He, S. D. Zhang, L. Zhang, F. Yang, Y. Q. Zhang, X. L. Huang and G. J. Wei, *Am. Mineral.*, 2022, **107**, 432–442.